Experimental and Theoretical Analyses of Axial Magnetic Coupling Under Steady-State and Transient Operations

Thierry Lubin, Smail Mezani, and Abderrezak Rezzoug

***Abstract*—This paper investigates the steady-state and transient performances of an axial magnetic coupling by using analytical formulas issued from an analytical model based on a 2-D approximation for the magnetic field distribution (mean radius model). From the magnetic field expression, simple analytical formulas are derived for computing the pull-out torque and the torsional stiffness of the coupling as a function of the geometrical parameters. Here, a special attention is given to the overload torque condition during the transient which leads to the loss of synchronism for the coupling. Moreover, radial and angular misalignment conditions are also studied. In order to study the accuracy of the proposed analytical model, the results are compared with those obtained from 3-D finite-element simulations and measurements.**

***Index Terms*—Analytical model, axial coupling, magnetic field, permanent magnets, pull-out torque, transient performance.**

NOMENCLATURE

R_1	Inner radius of the magnets.
R_2	Outer radius of the magnets.
R_e	Mean radius of the magnets.
h	Magnet thickness.
e	Air-gap thickness.
α	Permanent magnet (PM) pole-arc-to-pole-pitch ratio.
p	Pole-pair number.
δ	Torque angle.
B_r	Remanence of the permanent magnets.
K	Torsional stiffness.

I. INTRODUCTION

MAGNETIC couplings are used to transmit torque from a primary driver to a load without any mechanical contact. As the torque could be transmitted across a separation wall, magnetic couplings are well suited for use in isolated systems. Among the advantages of this type of coupling compared to mechanical couplings is the self-protection against the overload (pull-out torque). Moreover, magnetic couplings tolerate shaft misalignment.

As shown in Fig. 1, the studied axial magnetic coupling consists of two disks equipped with sector-shaped permanent magnets (rare-earth magnets) and separated by a small air gap. The magnets are axially magnetized and are arranged to obtain alternately north and south poles. Soft-iron yokes are used to close the flux. Through magnetic interaction, the torque applied to one disk is transferred through an air gap to the other disk.

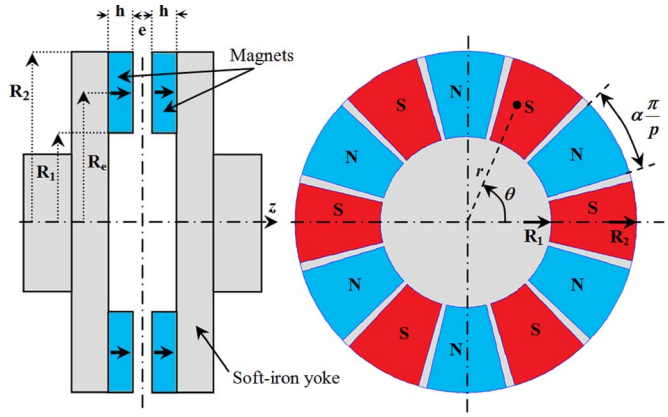

Fig. 1. Geometry of the studied axial magnetic coupling ($p = 6$).

In order to predict the steady-state and transient performances of magnetic couplings or PM actuators, an accurate knowledge of the air-gap flux density distribution is necessary. The flux density can be evaluated by analytical methods using 3-D formulation or approximate 2-D formulations [1]–[21] or by numerical techniques like finite elements [22]–[25]. Analytical methods generally require much less computational time than numerical ones and can provide a closed-form solution for the torque [5], [19], [20] which can be used in optimization codes.

While the steady-state performance of magnetic couplings or magnetic gears has been widely studied in the literature, only a little attention has been given to transient performances [26], [27], and experimental data are practically nonexistent [28], [29].

The purpose of this paper is to analyze the steady-state performance (pull-out torque) and the transient performance (start-up, sudden change in load torque, and overload conditions) of an axial magnetic coupling by using analytical formulas for the pull-out torque and the torsional stiffness. Compared to [29], a special attention is given here to overload torque conditions which lead to the loss of synchronism for the coupling. In order to study the accuracy of the proposed model, the results are compared with those obtained from 3-D finite-element simulations and measurements.

Manuscript received January 22, 2013; revised April 12, 2013, April 29, 2013, and May 16, 2013; accepted May 20, 2013. Date of publication June 4, 2013; date of current version February 7, 2014.

The authors are with the Groupe de Recherche en Electrotechnique et Electronique de Nancy, Université de Lorraine, 54506 Nancy, France (e-mail: thierry.lubin@univ-lorraine.fr).

Color versions of one or more of the figures in this paper are available online at http://ieeexplore.ieee.org.

Digital Object Identifier 10.1109/TIE.2013.2266087

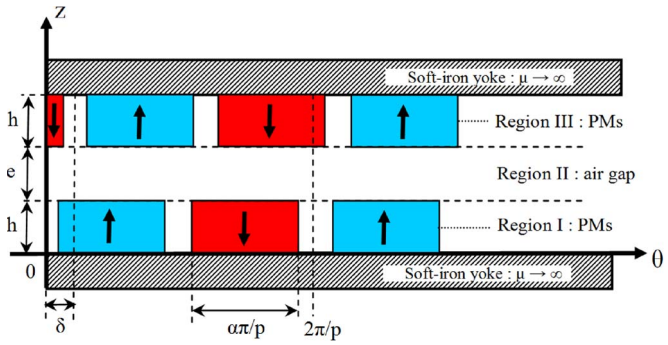

Fig. 2. Two-dimensional model of the axial magnetic coupling at the mean radius of the magnets $R_e = (R_1 + R_2)/2$.

II. Analytical Calculation of the Magnetic Field

Because of the 3-D nature of the magnetic field distribution, rigorous computation of the torque requires a full 3-D analysis [1]–[3], [7]. However, in order to simplify the analysis and to carry out simple formulas for the torque and the torsional stiffness, the 3-D problem of Fig. 1 is reduced to a 2-D one by introducing a cylindrical cutting surface at the mean radius of the magnets $R_e = (R_1 + R_2)/2$ on which the flux density will be computed. Fig. 2 shows the resulting 2-D model which makes the axial magnetic coupling equivalent to a linear magnetic coupling.

With this approach, we neglect the radial component of the magnetic field, and we consider that the axial and tangential components do not depend on the r-coordinate. Moreover, we consider that the iron yokes have infinite magnetic permeability (which gives homogeneous Neumann conditions on their boundaries). The magnets are axially magnetized with a relative recoil permeability $\mu_r = 1$.

The detailed developments for the magnetic field calculation in the different regions of Fig. 2 are given in [20] and will not be repeated here. In this paper, only the method and the most important relations are remembered. Compared to [20], the model has been simplified by only considering the first harmonic term of the magnetic field distribution. As it will be shown, this hypothesis leads to simple expressions for the axial and tangential components of the flux density in the air gap which allow computing very quickly the pull-out torque.

A. Magnetic Vector Potential in the Air Gap

A magnetic vector potential formulation has been used in [20] to study the problem shown in Fig. 2. With this formulation, we have to solve the following partial differential equations in the magnets and air-gap regions:

$$\frac{1}{R_e^2}\frac{\partial^2 A_i}{\partial \theta^2} + \frac{\partial^2 A_i}{\partial z^2} = -\frac{\mu_0}{R_e}\frac{\partial M_z}{\partial \theta} \quad \text{with} \quad i = I \text{ and } III \tag{1}$$

$$\frac{1}{R_e^2}\frac{\partial^2 A_{II}}{\partial \theta^2} + \frac{\partial^2 A_{II}}{\partial z^2} = 0 \quad \text{in the air-gap} \tag{2}$$

where μ_0 is the permeability of the vacuum and M_z is the axial magnetization of the magnets. Due to the periodicity of the magnetic field distribution, the studied domain has been limited by $0 \le \theta \le 2\pi/p$. The axial magnetization M_z can be expressed in Fourier's series and replaced in (1). If we consider only the first space harmonic term of the magnetization distribution, we can write

$$M_z(\theta) = \frac{4B_r}{\pi\mu_0}\sin\left(\alpha\frac{\pi}{2}\right)\sin\left(p(\theta-\delta)\right) \tag{3}$$

where δ (torque angle) is the relative angular position between the magnets of region I and region III as shown in Fig. 2. By considering the interface and boundary conditions for the magnetic field, we obtain the general solution of the magnetic vector potential in the air-gap region

$$\begin{aligned} A_{II}(\theta,z) = &\left(-a^{II}\frac{\cosh\left(k(z-h-e)\right)}{k\sinh(ke)}\right.\\ &\left.+b^{II}\frac{\cosh\left(k(z-h)\right)}{k\sinh(ke)}\right)\cos(p\theta)\\ &+\left(-c^{II}\frac{\cosh\left(k(z-h-e)\right)}{k\sinh(ke)}\right.\\ &\left.+d^{II}\frac{\cosh\left(k(z-h)\right)}{k\sinh(ke)}\right)\sin(p\theta) \end{aligned} \tag{4}$$

where $k = p/R_e$ and a^{II}, b^{II}, c^{II}, and d^{II} are the integration constants. These integration constants can be determined from the interface conditions between the regions as explained in [20].

B. Magnetic Flux Density in the Air Gap

The axial and tangential components of the magnetic flux density in the air gap can be deduced from the magnetic vector potential (4) using

$$B_{IIz} = -\frac{1}{R_e}\frac{\partial A_{II}}{\partial \theta} \quad \text{and} \quad B_{II\theta} = \frac{\partial A_{II}}{\partial z}. \tag{5}$$

To compute the pull-out torque from the Maxwell stress tensor, we have to know the flux density expression on a line in the air-gap region. The simplest expression for the flux density is obtained at $z = h + e/2$ (middle of the air gap). Moreover, with the first harmonic hypothesis, we know that the torque presents a sinusoidal characteristic, so we have to compute only its maximum value.

From (4) and (5) and after some calculus to obtain the values of the integration constants a^{II}, b^{II}, c^{II}, and d^{II}, the axial and tangential components of the magnetic flux density in the middle of the air gap for $\delta = \pi/2p$ are given by

$$\begin{aligned} B_{IIz}(\theta) = &\frac{4\sqrt{2}B_r}{\pi}\sin\left(\alpha\frac{\pi}{2}\right)\frac{\sinh(a)\cosh\left((1+\nu)a\right)}{\sinh\left(2(1+\nu)a\right)}\\ &\times\sin\left(p\theta-\frac{\pi}{4}\right) \end{aligned} \tag{6}$$

$$\begin{aligned} B_{II\theta}(\theta) = &\frac{4\sqrt{2}B_r}{\pi}\sin\left(\alpha\frac{\pi}{2}\right)\frac{\sinh(a)\sinh\left((1+\nu)a\right)}{\sinh\left(2(1+\nu)a\right)}\\ &\times\sin\left(p\theta-\frac{\pi}{4}\right) \end{aligned} \tag{7}$$

TABLE I
PARAMETERS OF THE STUDIED AXIAL COUPLING

Symbol	Quantity	value
R_1	Inner radius of the magnets	30 mm
R_2	Outer radius of the magnets	60 mm
R_e	Mean radius of the magnets	45 mm
h	Magnets thickness	7 mm
e	Air-gap length	variable
α	PMs pole-arc to pole-pitch ratio	0.9
p	Pole-pairs number	6
B_r	Remanence of the permanent magnets	1.25 T

where

$$a = p\frac{h}{R_e} \quad \text{and} \quad \nu = \frac{e}{2h}. \tag{8}$$

As expected, we can observe from (6) and (7) that the axial and tangential flux density waves are in phase when we consider the pull-out torque position.

By using (6) and (7), it is now possible to derive analytical formulas for the pull-out torque and for the torsional stiffness of the axial coupling. The next sections concern the analysis of the steady-state and transient performances of the coupling with experimental validations.

III. STEADY-STATE ANALYSIS

A. Pull-Out Torque Expression

The pull-out torque is obtained by the Maxwell stress tensor where a line at the middle of the air gap is taken as the integration path

$$T_{\max} = \frac{R_2^3 - R_1^3}{3\mu_0} \int_0^{2\pi} B_{II\theta}(\theta) B_{IIz}(\theta) d\theta. \tag{9}$$

Incorporating (6) and (7) into (9), we can derive a simple formula for the pull-out torque which depends directly on the geometrical parameters

$$T_e = T_{\max} \sin(p\delta) \tag{10}$$

with

$$T_{\max} = \frac{16}{3\pi} \frac{B_r^2}{\mu_0} R_2^3 \left(1 - \left(\frac{R_1}{R_2}\right)^3\right) \sin^2\left(\alpha \frac{\pi}{2}\right) \frac{\sinh^2(a)}{\sinh\left(2(1+\nu)a\right)}. \tag{11}$$

The formula (11) has been used in [20] for the optimal design of the coupling given in Table I.

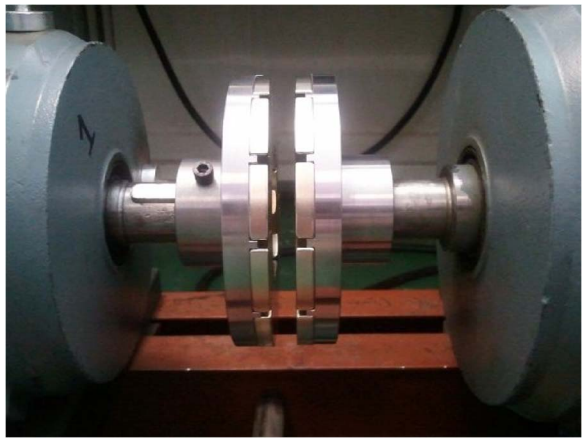

Fig. 3. Axial magnetic coupling prototype placed on the test bench ($e = 9.5$ mm).

B. 3-D Finite Element Simulations and Measurements

For the steady-state analysis, the formula (11) has been compared with both 3-D finite element method (FEM) simulations and experimental results. For the 3-D finite-element simulations, we have used COMSOL Multiphysics software. For the experimental validation, we have manufactured an axial magnetic coupling prototype using sector-type NdFeB magnets glued on iron yokes. The thickness of the iron yokes (1 cm) has been chosen to avoid magnetic saturation. The geometrical parameters of the prototype are those of Table I.

Fig. 3 shows the axial magnetic coupling placed on the test bench. The axial coupling is inserted between two electrical machines (dc motors of 3 kW and 1500 r/min). In Fig. 3, the air-gap value is $e = 9.5$ mm. The air-gap length has been set by inserting nonmagnetic plates of known thickness between the two disks. Fig. 4(a) and (b) show respectively a photograph and a block-scheme representation of the test bench arrangement for the static torque measurement. As shown in Fig. 4(b), the static torque was measured owing to weights (250 g, 500 g, and 1 kg) suspended to a rod ($l = 1$ m) locked to one rotor, with the other being fixed. The relative angular position δ was measured using an incremental encoder with a resolution of 4096 pulses/revolution (precision of 0.088°), and the data were transferred into a computer.

Fig. 5 shows the pull-out torque as a function of the air-gap length obtained with 3-D finite-element analysis and with the 2-D analytical model (11). As expected for this type of device, the 2-D analytical prediction gives higher values for the pull-out torque as compared to the 3-D finite element (FE) analysis [20]. This is mainly due to the 3-D effects which are not taken into account in the proposed model (the radial dependence of the magnetic field is not considered). The error on the pull-out torque prediction ranges from 22% for $e = 2$ mm to 31% for $e = 10$ mm.

In order to analyze the error on the torque prediction of the 2-D model, a parametric study has been carried out. For a magnet thickness $h = 7$ mm and an air gap $e = 4$ mm, we vary R_1, R_2, and p in the following intervals:

1) $R_2 = [40$ mm to 140 mm$]$ with a step of 20 mm (six values);

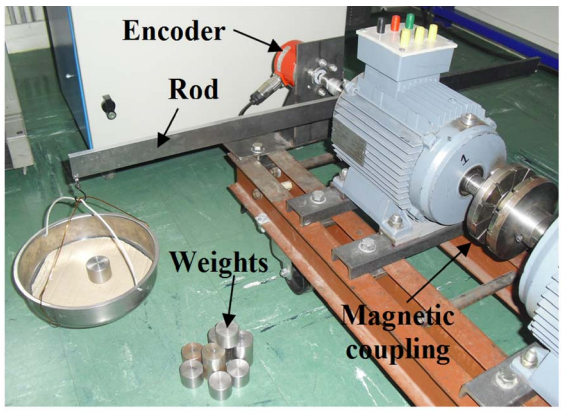

(a)

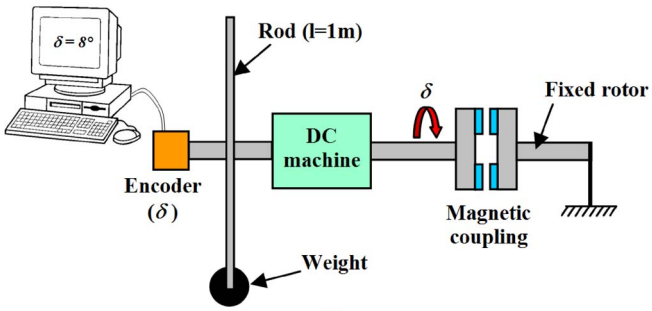

(b)

Fig. 4. Experimental setup for the static torque measurement. (a) Photograph. (b) Block-scheme representation (top view).

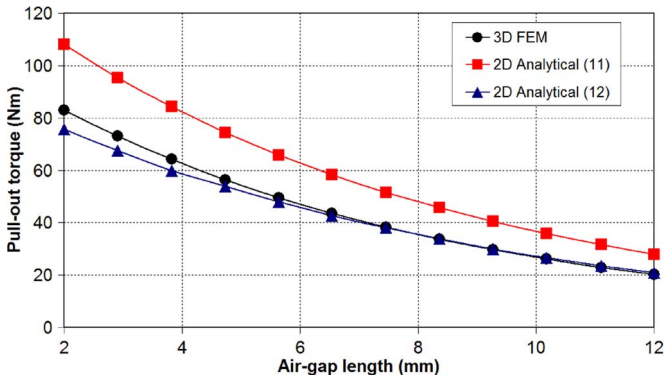

Fig. 5. Pull-out torque versus the air-gap length: Three-dimensional FEM and 2-D analytical results.

2) $R_1 = [0.2 \times R_2$ to $0.8 \times R_2]$ with a step of $0.1 \times R_2$ (seven values);
3) $p = [2$ to $8]$ with a step of 1 (seven values).

This corresponds to 294 combinations.

Then, for each value of R_2, we have 49 evaluations (3-D FE) of the pull-out torque T_{3D}, with the maximal value being denoted as T_{3D-max}. Among these 49 calculations, we have only considered the representative values for which $T_{3D}/T_{3D-max} > 0.7$. Indeed, we always look, in practice, to the most favorable configurations which maximize the torque.

A nondimensional number $\lambda = \pi(R_2 + R_1)/(2p(R_2 - R_1))$ is introduced. It allows comparing the magnet height $(R_2 - R_1)$ and the mean pole pitch $\pi(R_2 + R_1)/2p$.

We have defined a correction factor of the 2-D model by $k_c = T_{max}/T_{3D}$, where T_{max} is given by (11). Fig. 6 gives the

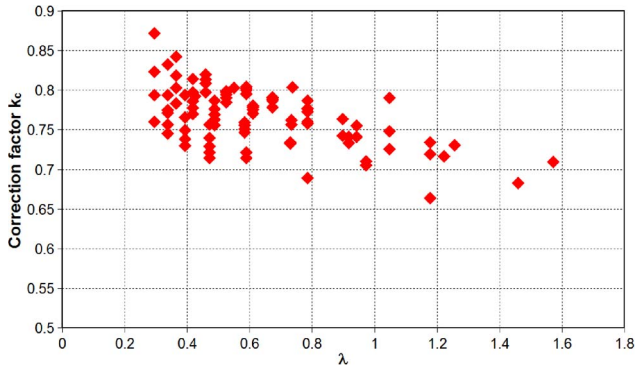

Fig. 6. Correction factor k_c (for $e = 4$ mm).

variation of k_c versus λ. It can be seen that the values of k_c range between 0.7 and 0.8 for the most representative cases. Furthermore, one can see that the optimal values of λ that maximize the torque transmission capabilities of the coupling are between 0.3 and 0.8. Notice that these optimal values of λ can also be predicted with the formula (11) as indicated in [20].

Hence, for engineering purposes, a correction factor k_c, based on the results of Fig. 6, can be introduced to improve the precision of the torque formula (11)

$$T_{max\,c} = k_c T_{max} \quad \text{with} \quad k_c \approx 0.75 \tag{12}$$

where T_{max} is given by (11). As it can be observed in Fig. 5, a simple correction coefficient in the analytical torque expression leads to acceptable results, whatever the air-gap length.

Fig. 7 shows the comparison between the measured values of the static torque (see Fig. 4) and the calculated ones by using the 2-D analytical models and 3-D FEM. Here, four values of the air-gap length were considered ($e = 4$ mm, $e = 9.5$ mm, $e = 13$ mm, and $e = 20$ mm). It can be observed in Fig. 7 that the measurements are in good agreement with both the 3-D FE simulations and the 2-D corrected analytical model given by (12).

C. Tolerance to Radial and Angular Misalignments

Fig. 8 shows the influence of the radial and angular misalignments on the static torque of the designed coupling (results obtained with 3-D FE analysis). It can be seen that a radial misalignment of $d = 10$ mm leads to a reduction of the maximum torque of about 11% compared to the case where $d = 0$. On another hand, an angular displacement of $\beta = 1°$ leads to a reduction of about 25% of the maximum torque compared to the healthy situation $(\beta = 0)$. It can be concluded that the torque transmission capabilities of the coupling are more sensitive to angular misalignments.

IV. Transient Analysis

A. Torsional Stiffness Expression

In the transient analysis of magnetic couplings or magnetic gears [26]–[29], one of the most important parameters is the torsional stiffness K (in newton meters per radian). It is equal to the initial slope of the torque versus position curves shown in Fig. 7. This coefficient depends on the geometrical parameters

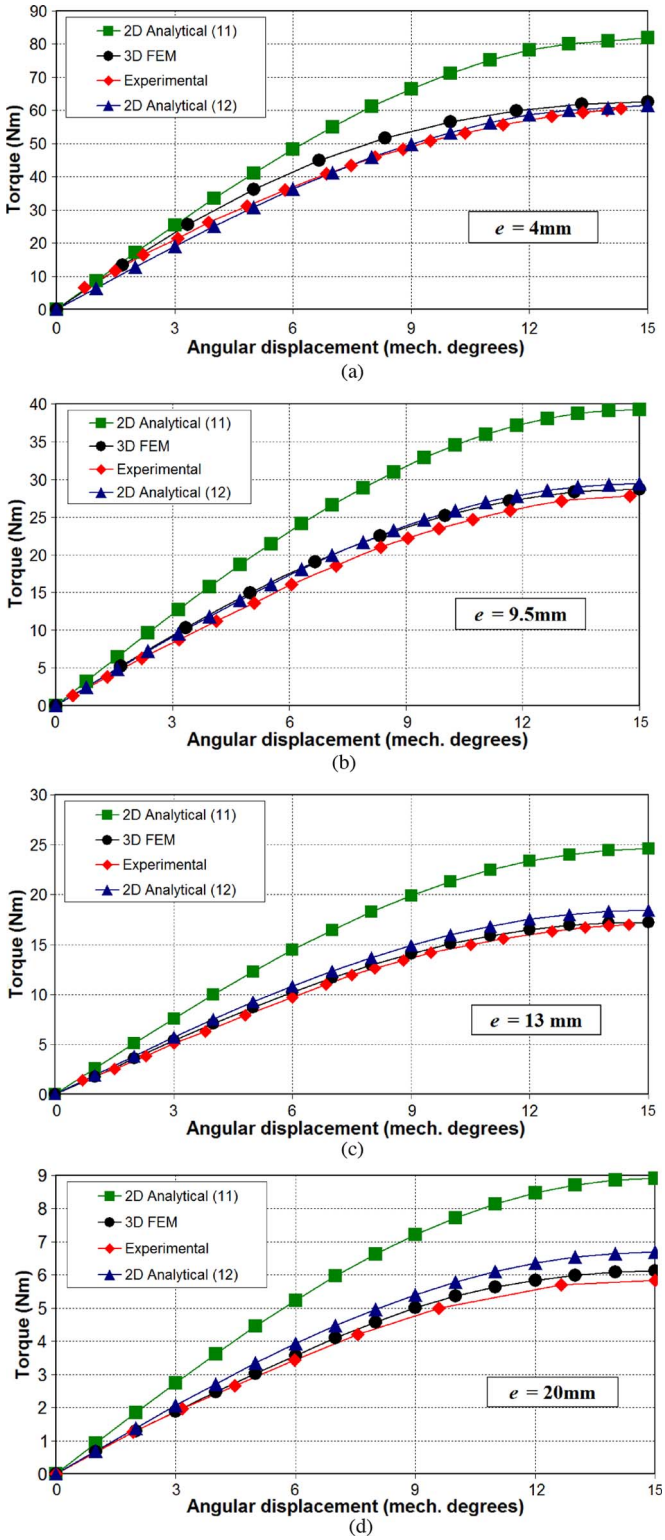

Fig. 7. Measured and computed static torques versus the angular displacement δ: (a) $e = 4$ mm, (b) $e = 9.5$ mm, (c) $e = 13$ mm, and (d) $e = 20$ mm.

of the coupling and, more particularly, on the air-gap value e. From (10) and (12), we can obtain an analytical expression for K

$$K = pT_{\max c}. \tag{13}$$

Fig. 9 shows the variation of the torsional stiffness K versus the air-gap length. As expected, the coefficient K decreases

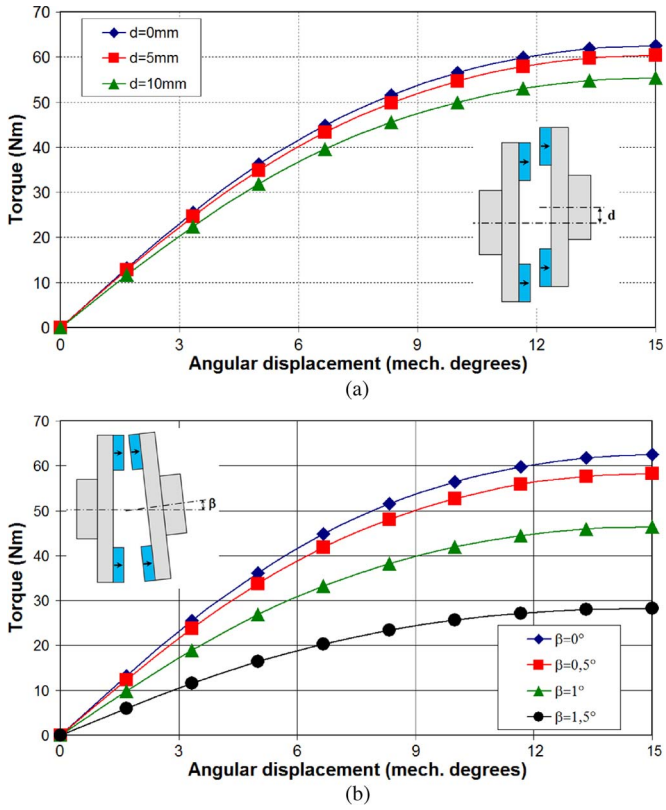

Fig. 8. Effects of misalignment on the static torque for $e = 4$ mm: (a) Radial misalignment and (b) angular misalignment.

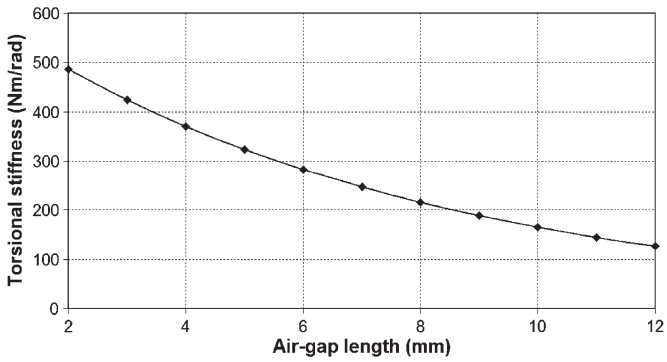

Fig. 9. Torsional stiffness (K) versus the air-gap length for the studied magnetic coupling.

with the air-gap length (the coupling is more elastic with a large air gap). For an air-gap value of 4 mm, the torsional stiffness of the studied magnetic coupling is around 370 N · m/rad. For comparison, rigid or semiflexible mechanical couplings present a torsional stiffness of more than 5000 N · m/rad.

B. Equations of Motion

The transient analysis of the magnetic coupling is obtained from the equation of motion for rotating rigid bodies. Fig. 10 shows the scheme of the test bench. The dc motor rotates at Ω_m, and the load runs at Ω_l.

In steady-state condition, the two speeds are the same. Two encoders (4096 pulses/revolution) have been placed on the test bench to measure the relative angular position between the dc

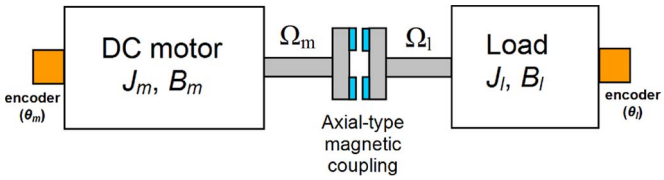

Fig. 10. Scheme of the test bench.

motor and the load and to measure the speed on both sides of the coupling during the transient.

The motion equations are given by

$$J_m \frac{d\Omega_m}{dt} + B_m \Omega_m = T_{\mathrm{DC}} - T_e$$
$$J_l \frac{d\Omega_l}{dt} + B_l \Omega_l = T_e - T_{\mathrm{load}} \tag{14}$$

where J_m and B_m denote the total moment of inertia and the coefficient of friction of the dc motor and one part of the axial coupling and J_l and B_l denote the total moment of inertia and the coefficient of friction of the other part of the axial coupling and the load. T_{DC} is the dc motor torque, and T_{load} is the external load torque. The torque of the magnetic coupling (10) and (12) can be rewritten as follows:

$$T_e = T_{\max c} \sin\left(p(\theta_m - \theta_l)\right) \tag{15}$$

where $\Omega_m = d\theta_m/dt$ and $\Omega_l = d\theta_l/dt$.

C. Sudden Application of Load Torque

In order to study the transient behavior of the coupling, a first test consists of blocking one part of the magnetic coupling (the dc motor part is locked, i.e., $\theta_m = 0$ and $\Omega_m = 0$) and applying a sudden variation on the load torque (supplementary weight from a wire attached at the end of a rod as shown in Fig. 4). In this case, the motion equation (14) becomes

$$J_l \frac{d^2\theta_l}{dt^2} + B_l \frac{d\theta_l}{dt} = -T_{\max c} \sin(p\theta_l) + T_{\mathrm{load}}. \tag{16}$$

If we consider a small variation of the load torque ΔT_{load} and a value of θ_l near zero, (16) can be rewritten as a second-order linear differential equation

$$J_l \frac{d^2\theta_l}{dt^2} + B_l \frac{d\theta_l}{dt} + K\theta_l = \Delta T_{\mathrm{load}} \tag{17}$$

where K is given by (13). We can define the damping ratio ξ and the oscillation period T as

$$\xi = \frac{B_l}{2\sqrt{K J_l}} \quad T = 2\pi\sqrt{\frac{J_l}{K}}. \tag{18}$$

The load torque variation and the moment of inertia J_l (obtained by Huygens' theorem) depend on the total weight $m + \Delta m$ attached to the rod (rod of length $l = 1$ m) as

$$\Delta T_{\mathrm{load}} = \frac{l}{2} g \Delta m \quad \text{and} \quad J_l = J + (m + \Delta m)\left(\frac{l}{2}\right)^2 \tag{19}$$

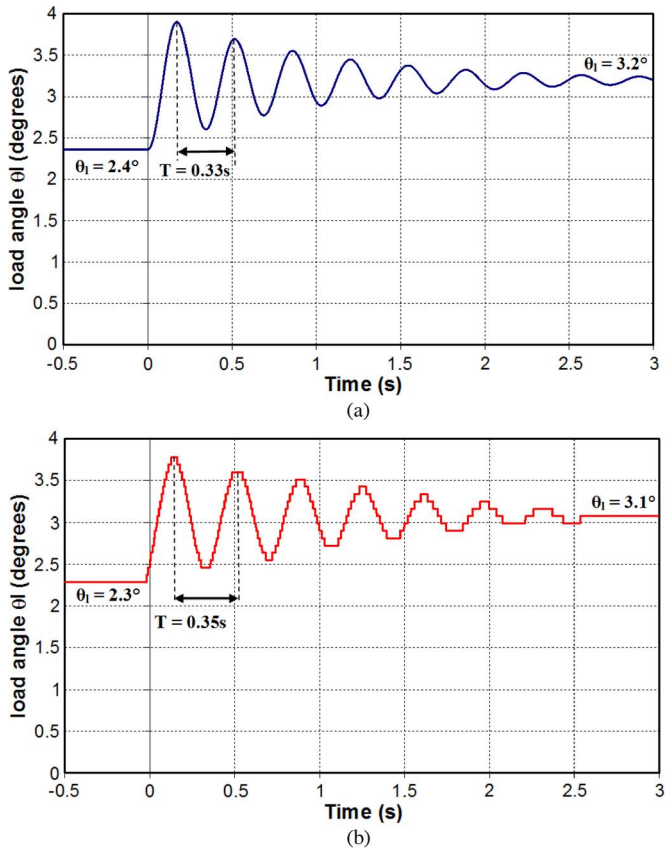

Fig. 11. Load angle oscillations due to a sudden variation of the load torque ($\Delta T_{\mathrm{load}} = 5$ N · m) for $e = 4$ mm and $K = 370$ N · m/rad: (a) Simulation result and (b) experimental result.

where $g = 9.81$ m · s^{-2}, J is the load inertia without weight ($J = 0.01$ kg · m^2), m is the initial weight, and Δm is the supplementary weight applied at $t = 0$ s.

Fig. 11 shows the variation of the load angle θ_l (simulation results obtained with (17) and experimental results) when we apply a load torque step of 5 N · m at $t = 0$ s that corresponds to a weight of around $\Delta m = 1$ kg (the initial torque is fixed to 14.7 N · m, i.e., $m = 3$ kg). The moment of inertia J_l given by (19) is then equal to 1.01 kg · m^2. The torsional stiffness of the magnetic coupling is $K = 370$ N · m/rad (air gap of 4 mm). The oscillation period can be estimated by (18) at $T = 0.33$ s that is close to the experimental results ($T = 0.35$ s) given in Fig. 11. As shown in Fig. 11, the initial and final load angles can also be predicted with a very good precision by using the analytical model ($\sin\theta_l = T_{\mathrm{load}}/T_{\max c}$).

D. Transient Performance During Start-Up

The transient start-up performance is assessed by running the dc motor from standstill (at $t = 0$ s) to the speed of 400 r/min under no-load condition. Figs. 12–14 show the speed responses for three values of the air-gap length ($e = 4$ mm, $e = 13$ mm, and $e = 20$ mm). The simulation results have been computed with (14) and (15). Experimental and simulation results show clearly that there are speed oscillations with time delays between the two rotors of the magnetic coupling. As expected from (18), the oscillation period T increases when the torsional stiffness of the coupling decreases (i.e., the air gap

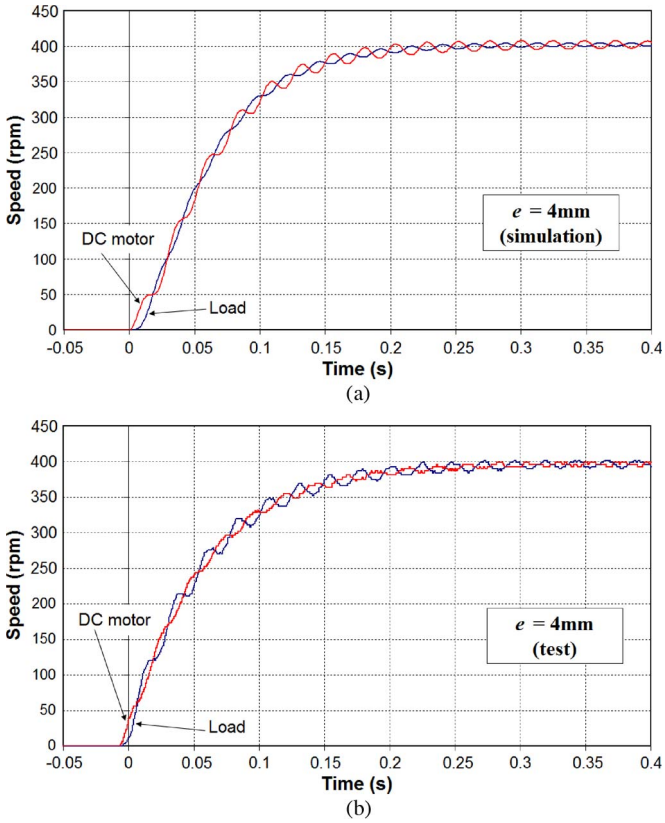

Fig. 12. Speed responses with torsional stiffness $K = 370$ N · m/rad ($e = 4$ mm): (a) Simulation result and (b) experimental result.

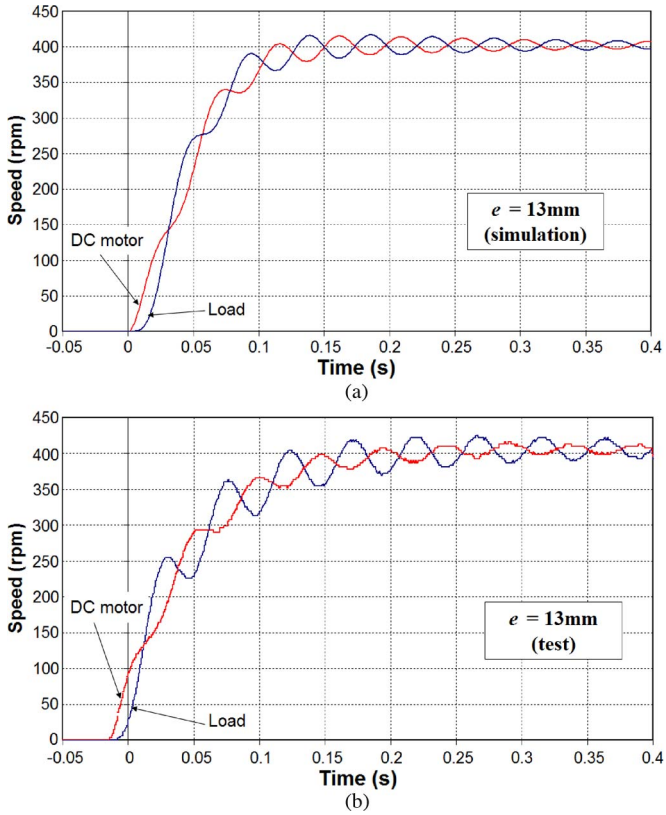

Fig. 13. Speed responses with torsional stiffness $K = 105$ N · m/rad ($e = 13$ mm): (a) Simulation result and (b) experimental result.

increases) as shown in Figs. 12–14. These speed oscillations have to be taken into account for servomechanism applications.

During the starting, there are some power losses in the permanent magnets and iron yokes (eddy current). This is due to the speed difference between the two rotors. The eddy current causes additional "damping" torque (asynchronous torque) which can be included in the transient analysis of the coupling [28] by increasing the damping ratio (18). The computation of the eddy current could be done analytically with the resistance-limited assumption [30], [31] or by finite-element simulations. Anyway, this study is complex and is outside the objective of this paper.

Fig. 15 shows the variation of the angular displacement between the two sides of the coupling $\Delta\theta = \theta_m - \theta_l$ during start-up under no-load condition (corresponding to the speed variations given in Fig. 14). As shown in Fig. 15, $\Delta\theta$ reaches a value of 15.7° (at $t = 0.025$ s) which is slightly greater than its maximum value before instability ($\Delta\theta_{\max} = 15°$ for $p = 6$). However, we can observe that the coupling does not lose the synchronism for this test. This can be explained by the additional torque (asynchronous torque) due to eddy current as indicated previously. After the transient, the displacement angle reduces to a zero mean value for this no-load test, as shown in Fig. 15.

Another test with a larger speed variation (standstill to 725 r/min) has been performed, and the results (simulation and experimental) are given in Fig. 16. For this test, the air-gap value is fixed to $e = 20$ mm. It can be seen in Fig. 16 that the synchronism is lost by this abrupt start-up of the dc motor which

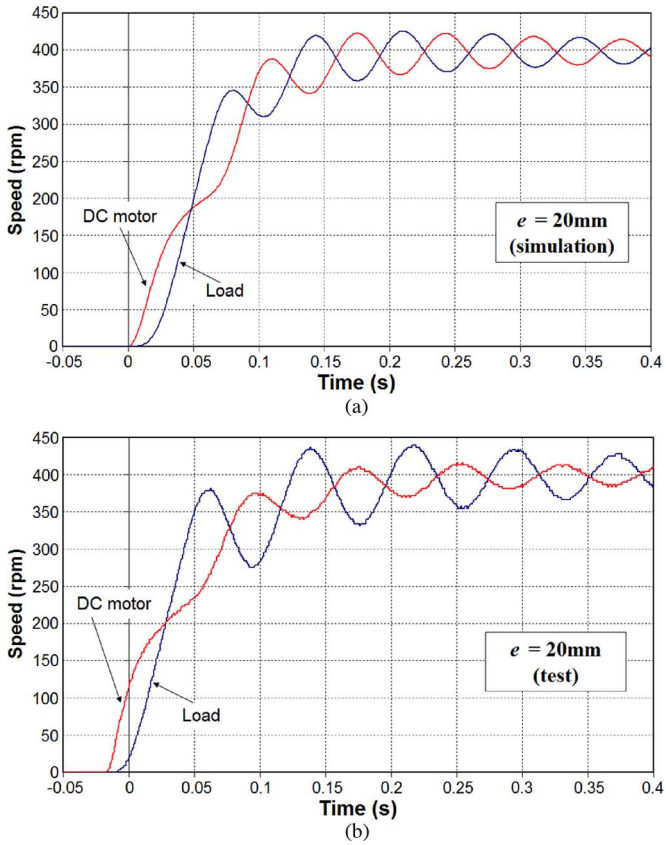

Fig. 14. Speed responses with torsional stiffness $K = 42$ N · m/rad ($e = 20$ mm): (a) Simulation result and (b) experimental result.

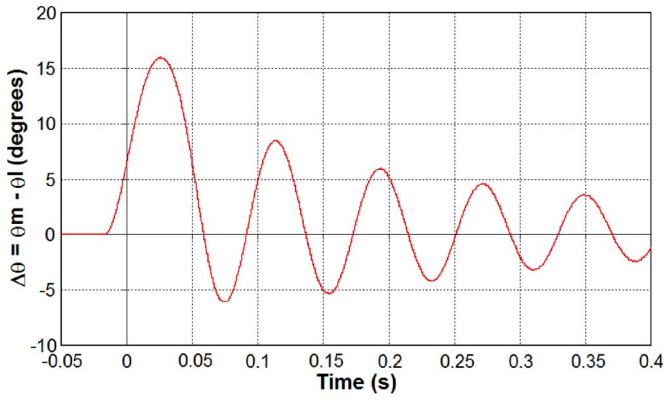

Fig. 15. Angular displacement between the two sides of the coupling during starting under no-load condition: Experimental result ($e = 20$ mm).

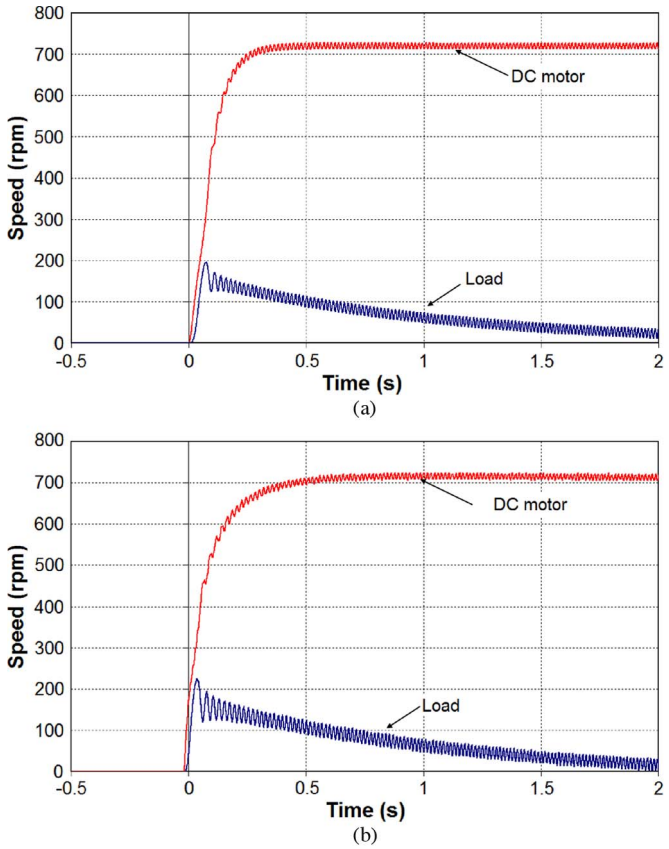

Fig. 16. Loss of synchronism caused by an abrupt start-up of the dc motor (from standstill to 725 r/min): (a) Simulation and (b) experimental results.

causes the load to stall. It is important to keep in mind this problem when designing the coupling. Of course, for a lower value of the air gap, the synchronism would be kept. One can observe in Fig. 16 that the simulation and test results are in close agreement.

E. Transient Performance With Load Variation

The transient performance with an abrupt application of a load torque is now studied. Before the load torque is applied, the dc motor is in steady-state condition and rotates with a speed of around 750 r/min (under no-load condition). Two cases are interesting to study: torque variation lower or greater than the

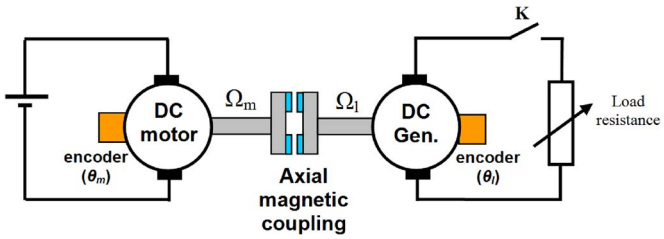

Fig. 17. Test bench arrangement for sudden application of load torque.

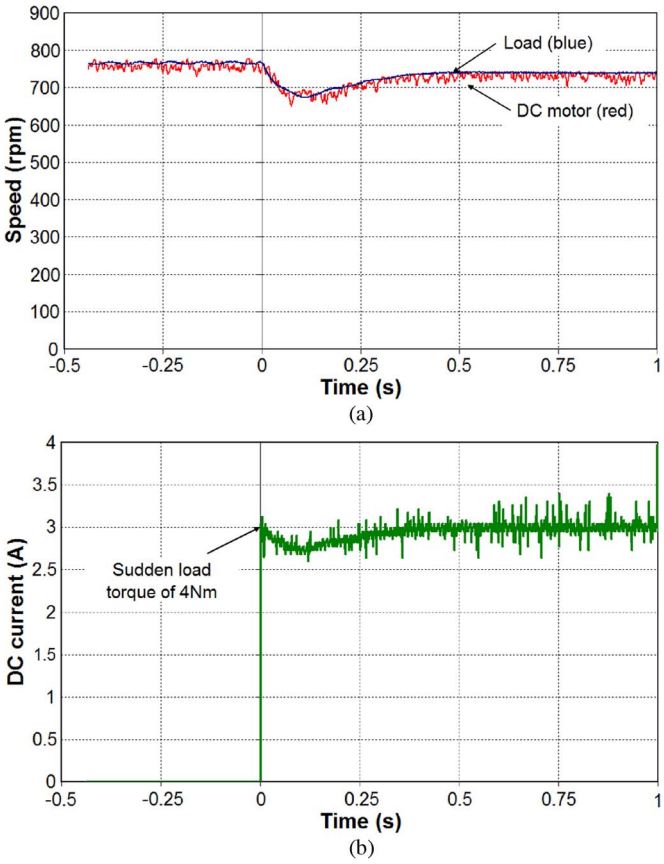

Fig. 18. Speed responses to a sudden load torque of 4 N · m with $e = 20$ mm: (a) Motor and load speeds and (b) current in the dc generator (experimental).

pull-out torque. In one case, we do not lose the synchronism, while in the other case, the synchronism will be lost. For these tests, the air-gap value is fixed to $e = 20$ mm that corresponds to a pull-out torque of around 6 N · m as shown in Fig. 7(d). A schematic view of the test bench arrangement is given in Fig. 17. A dc generator is used to apply the sudden load torque by connecting a resistance to its terminal armature winding.

First of all, a sudden load torque of 4 N · m is applied to the system at $t = 0$ s as shown in Fig. 18 (a load torque of 4 N · m corresponds to a dc current in the generator of 3 A, with the torque coefficient of the dc generator being equal to 1.35 N · m/A). This load disturbance corresponds to 2/3 of the load which causes the synchronism loss. Fig. 18 shows the speed responses and the dc current in the generator. It can be seen that the settling time of the dc current is very fast compared to the speed variations. After a transient of around 0.3 s, the two speeds are stable again and are synchronous. For this test, the synchronism is not lost.

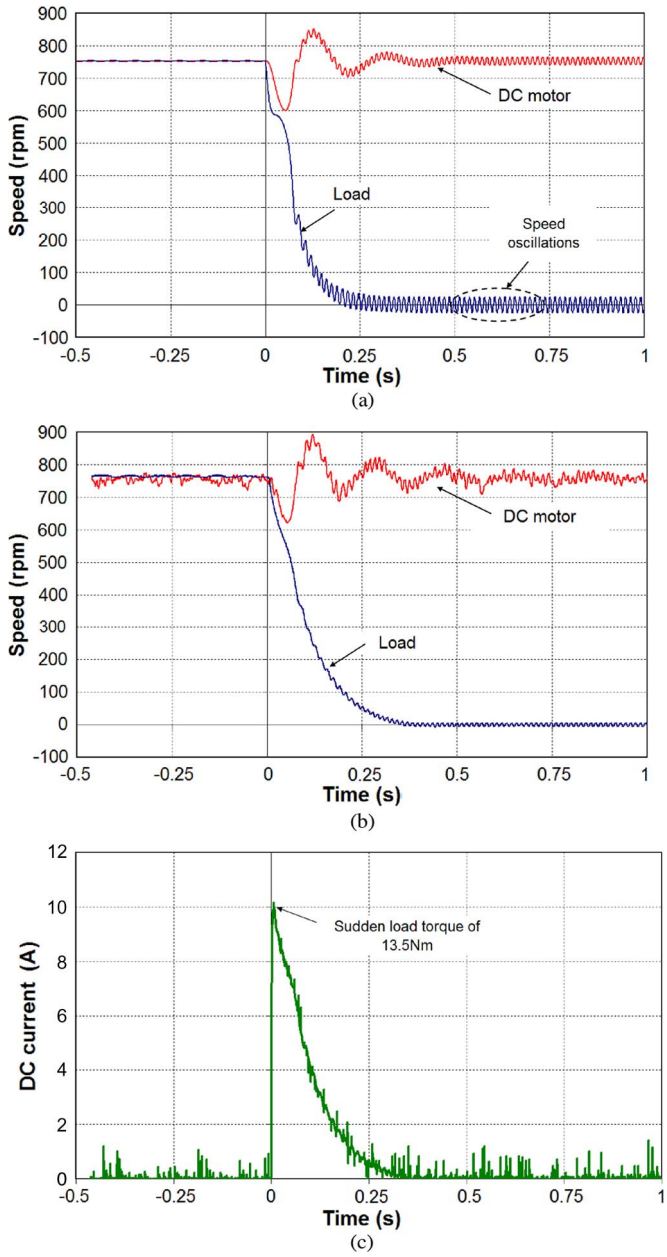

Fig. 19. Speed responses to an overload condition (sudden load torque of 13.5 N · m with $e = 20$ mm): (a) Simulation, (b) experimental results, and (c) electrical current in the dc generator (experimental).

Fig. 19 shows the speed responses (simulation and experimental results) that follow a sudden application of a load torque of 13.5 N · m at $t = 0$ s (dc current of 10 A) which is sufficient to cause the synchronism loss (overload condition).

As shown in Fig. 19, the speed of the dc motor is maintained at around 750 r/min (after some oscillations) while the load side of the coupling stops. This test clearly shows the overload self-protection of the magnetic coupling. On Fig. 19(a), we can observe speed oscillations on the load side around a zero mean value. This "sinusoidal" speed oscillation is caused by the torque variation given by (15) after overloading. The oscillation frequency can be predicted easily as the product of the dc motor speed in revolutions per second $(750/60 = 12.5$ rps) by the number of pole pairs of the magnetic coupling $(p = 6)$. This gives a frequency of 75 Hz [around 19 periods between 0.5 and 0.75 s as shown in Fig. 19(a)]. This frequency is also present in the dc motor speed. This signal can be used by a controller to detect an overloading condition as it is shown in [28] for magnetic gears.

V. Conclusion

By using analytical formulas for the pull-out torque and for the torsional stiffness, both the steady-state and transient performances of an axial magnetic coupling have been studied in this paper. The proposed 2-D analytical model, which is very fast to perform, presents some lack of accuracy compared to 3-D finite-element simulations and experimental results (error of around 25% on the pull-out torque prediction). To improve the predictions, a correction factor k_c has been introduced in the pull-out torque formula. Through detailed transient analysis and experimental results, we have shown that the magnetic coupling causes speed oscillations with time delays between the two rotors during start-up. This is due to the low value of the torsional stiffness inherent to magnetic couplings. This must be taken into account for servomechanism applications and every transient behavior. Finally, we have verified by simulation and by tests the overload self-protection of the magnetic coupling.

VI. Acknowledgement

The authors would like to thank J.-Y. Morel and his team from the mechanical workshop at École Nationale Supérieure d'Electricité et de Mécanique for their assistance in the manufacture of the magnetics coupling.

References

[1] A. Rezzoug and F. M. Sargos, "Three dimensional field computation of charged sectors: A semi-analytical method," *IEEE Trans. Magn.*, vol. MAG-23, no. 4, pp. 1978–1984, Jul. 1987.
[2] J. P. Yonnet, S. Hemmerlin, E. Rulliere, and G. Lemarquand, "Analytical calculation of permanent magnet couplings," *IEEE Trans. Magn.*, vol. 29, no. 6, pp. 2932–2934, Nov. 1993.
[3] E. P. Furlani, R. Wang, and H. Kusnadi, "A three-dimensional model for computing the torque of radial couplings," *IEEE Trans. Magn.*, vol. 31, no. 5, pp. 2522–2526, Sep. 1995.
[4] Y. D. Yao, G. J. Chiou, D. R. Huang, and S. J. Wang, "Theoretical computations for the torque of magnetic coupling," *IEEE Trans. Magn.*, vol. 31, no. 3, pp. 1881–1884, May 1995.
[5] J. F. Charpentier and G. Lemarquand, "Optimal design of cylindrical air-gap synchronous permanent magnet couplings," *IEEE Trans. Magn.*, vol. 35, no. 2, pp. 1037–1046, Mar. 1999.
[6] P. Pfister and Y. Perriard, "Very-high-speed slotless permanent-magnet motors: Analytical modeling, optimization, design, and torque measurement methods," *IEEE Trans. Ind. Electron.*, vol. 57, no. 1, pp. 296–303, Jan. 2010.
[7] R. Ravaud, V. Lemarquand, and G. Lemarquand, "Analytical design of permanent magnet radial couplings," *IEEE Trans. Magn.*, vol. 46, no. 11, pp. 3860–3865, Nov. 2010.
[8] R. P. Praveen, M. H. Ravichandran, V. T. S. Achari, V. P. J. Raj, G. Madhu, and G. R. Bindu, "A novel slotless Halbach-array permanent-magnet brushless dc motor for spacecraft applications," *IEEE Trans. Ind. Electron.*, vol. 59, no. 9, pp. 3553–3560, Sep. 2012.
[9] J. P. C. Smeets, T. T. Overboom, J. W. Jansen, and E. A. Lomonova, "Modeling framework for contactless energy transfer systems for linear actuators," *IEEE Trans. Ind. Electron.*, vol. 60, no. 1, pp. 391–399, Jan. 2013.
[10] F. Weizhong and P. C. K. Luk, "Torque ripple reduction of a direct-drive permanent-magnet synchronous machine by material-efficient axial pole pairing," *IEEE Trans. Ind. Electron.*, vol. 59, no. 6, pp. 2601–2611, Jun. 2012.

[11] A. Di Gerlando, G. M. Foglia, and M. F. Iacchetti, "FEM2D based analytical model of the air gap magnetic field in surface PM synchronous machines," in *Proc. 20th ICEM*, Sep. 2012, pp. 2832–2838.
[12] L. Belguerras, L. Hadjout, T. Lubin, S. Mezani, and A. Rezzoug, "Analytical computation of flux concentration PM machines: Study of the influence of the magnets shape," in *Proc. 20th ICEM*, Sep. 2012, pp. 2752–2758.
[13] L. J. Wang, L. Hu, K. M. Lee, X. D. Ruan, and X. Fu, "Analytical magnetic field and driving force models based on measured boundary conditions for industrial coriolis mass flowmeters," *IEEE Trans. Ind. Electron.*, vol. 59, no. 12, pp. 4753–4760, Dec. 2012.
[14] W. Xie, G. Dajaku, and D. Gerling, "Analytical method for predicting the air-gap flux density of dual-rotor permanent-magnet (DRPM) machine," in *Proc. 20th ICEM*, Sep. 2012, pp. 2766–2771.
[15] K. Boughrara, R. Ibtiouen, and O. Touhami, "Exact analytical prediction of magnetic field in a hybrid and wound excitation synchronous machine," in *Proc. 20th ICEM*, Sep. 2012, pp. 2818–2824.
[16] L. J. Wu, Z. Q. Zhu, D. A. Staton, M. Popescu, and D. Hawkins, "Comparison of analytical models of cogging torque in surface-mounted PM machines," *IEEE Trans. Ind. Electron.*, vol. 59, no. 6, pp. 2414–2425, Jun. 2012.
[17] T. Lubin, S. Mezani, and A. Rezzoug, "2D analytical calculation of magnetic field and electromagnetic torque for surface-inset permanent magnet motors," *IEEE Trans. Magn.*, vol. 48, no. 6, pp. 2080–2091, Jun. 2012.
[18] J. Krotsch and B. Piepenbreier, "Radial forces in external rotor permanent magnet synchronous motors with non-overlapping windings," *IEEE Trans. Ind. Electron.*, vol. 59, no. 5, pp. 2267–2276, May 2012.
[19] J. Fontchastagner, Y. Lefèvre, and F. Messine, "Some co-axial magnetic couplings designed using an analytical model and an exact global optimization code," *IEEE Trans. Magn.*, vol. 45, no. 3, pp. 1458–1461, Mar. 2009.
[20] T. Lubin, S. Mezani, and A. Rezzoug, "Simple analytical expressions for the force and torque of axial magnetic couplings," *IEEE Trans. Energy. Convers.*, vol. 27, no. 2, pp. 536–546, Jun. 2012.
[21] N. Niguchi and K. Hirata, "Cogging torque analysis of magnetic gear," *IEEE Trans. Ind. Electron.*, vol. 59, no. 5, pp. 2189–2197, May 2012.
[22] C. Ferreira and J. Vaidya, "Torque analysis of permanent magnet coupling using 2D and 3D finite elements methods," *IEEE Trans. Magn.*, vol. 25, no. 4, pp. 3080–3082, Jul. 1989.
[23] W. Wu, H. C. Lovatt, and J. C. Dunlop, "Analysis and design optimisation of magnetic couplings using 3D finite element modelling," *IEEE Trans. Magn.*, vol. 33, no. 5, pp. 4083–4094, Sep. 1997.
[24] R. Wang, E. P. Furlani, and Z. J. Cendes, "Design and analysis of a permanent magnet axial coupling using 3D finite element field computations," *IEEE Trans. Magn.*, vol. 30, no. 4, pp. 2292–2295, Jul. 1994.
[25] Y. Kano, T. Kosaka, and N. Matsui, "A simple nonlinear magnetic analysis for axial-flux permanent-magnet machines," *IEEE Trans. Ind. Electron.*, vol. 57, no. 6, pp. 2124–2133, Jun. 2010.
[26] K. T. Chau, D. Zhang, J. Z. Jiang, and L. Jian, "Transient analysis of coaxial magnetic gears using finite element comodeling," *J. Appl. Phys.*, vol. 103, no. 7, pp. 07F101-1–07F101-3, Apr. 2008.
[27] N. W. Franck, S. Pakdelian, and H. A. Toliyat, "Passive suppression of transient oscillations in the concentric planetary magnetic gear," *IEEE Trans. Energy. Convers.*, vol. 26, no. 3, pp. 933–939, Sep. 2011.
[28] R. G. Montague, C. M. Bingham, and K. Atallah, "Servo control of magnetic gears," *IEEE/ASME Trans. Mechatronics*, vol. 17, no. 2, pp. 269–278, Apr. 2012.
[29] T. Lubin, S. Mezani, and A. Rezzoug, "Steady-state and transient analysis of an axial flux magnetic coupling," in *Proc. 20th ICEM*, Sep. 2012, pp. 1443–1449.
[30] H. Toda, Z. Xia, J. Wang, K. Atallah, and D. Howe, "Rotor eddy-current loss in permanent magnet brushless machine," *IEEE Trans. Magn.*, vol. 40, no. 4, pp. 2104–2106, Jul. 2004.
[31] L. Alberti, E. Fornasiero, N. Bianchi, and S. Bolognani, "Rotor losses measurements in an axial flux permanent magnet machine," *IEEE Trans. Energy. Convers.*, vol. 26, no. 2, pp. 639–645, Jun. 2011.

Thierry Lubin was born in Sedan, France, in 1970. He received the M.S. degree from the University Pierre et Marie Curie, Paris, France, in 1994 and the Ph.D. degree from the University Henri Poincaré, Nancy, France, in 2003.

He is currently a Lecturer of Electrical Engineering with the Groupe de Recherche en Electrotechnique et Electronique de Nancy, University of Lorraine, Nancy. His research interests include the modeling and control of electrical machines and applied superconductivity in electrical devices.

Smail Mezani was born in Algiers, Algeria, in 1974. He received the engineer diploma and the magister degree from the University of Sciences and Technology Houari Boumediene, Algiers, Algeria, in 1996 and 1999, respectively, and the Ph.D. degree from the Institut National Polytechnique de Lorraine, Vandoeuvre Les Nancy, France, in 2004.

He is currently a Lecturer with the University of Lorraine, Nancy, France, in the Groupe de Recherche en Electrotechnique et Electronique de Nancy, where his research interests include applications of superconductors in electromechanical devices.

Abderrezak Rezzoug received the electrical engineer degree from École Nationale Supérieure d'Electricité et de Mécanique Institut National Polytechnique de Lorraine, Nancy, France, in 1972 and the Dr. Ing. diploma and the Ph.D. degree from INPL in 1979 and 1987, respectively.

After working at the INPL as an Assistant Professor until 1991, he became a Professor of Electrical Engineering with the University of Lorraine, Nancy, France. As a member of the Groupe de Recherche en Electrotechnique et Electronique de Nancy, his main subjects of research concern superconducting applications to electrical devices and the control and diagnosis of electrical machines.